Korean J. Chem. Eng., 33(4), 1352-1361 (2016)
DOI: 10.1007/s11814-014-0334-6

pISSN: 0256-1115
eISSN: 1975-7220

Optimization of cationic dye adsorption on activated spent tea: Equilibrium, kinetics, thermodynamic and artificial neural network modeling

Ali Akbar Babaei[*,], Alireza Khataee[***], Elham Ahmadpour[****], Mohsen Sheydaei[***], Babak Kakavandi[**], and Zahra Alaee[*****,†]**

*Environmental Technologies Research Center, Ahvaz Jundishapur University of Medical Sciences, Ahvaz, Iran
**Department of Environmental Health Engineering, School of Public Health, Ahvaz Jundishapur University of Medical Sciences, Ahvaz, Iran
***Research Laboratory of Advanced Water and Wastewater Treatment Processes, Department of Applied Chemistry, Faculty of Chemistry, University of Tabriz, Tabriz, Iran
****Department of Environment and Occupational Health, Deputy of Health, Ahvaz Jundishapur University of Medical Sciences, Ahvaz, Iran
*****Student Research Committee, Ahvaz Jundishapur University of Medical Sciences, Ahvaz, Iran
(*Received 30 June 2014 • accepted 13 November 2014*)

Abstract−Activated spent tea (AST) was prepared and characterized by using different techniques such as BET, FTIR and SEM. It is used for methylene blue (MB) dye removal from aqueous solution in a batch system. Experimental results showed that natural basic pH, increased initial dye concentration, and high temperature favored the adsorption. Analysis based on the artificial neural network (ANN) indicated that the adsorbent dose and time with the relative importance of 30.03 and 35.44%, respectively, appeared to be the most influential parameters in the MB adsorption. The adsorption of MB was relatively fast and the Avrami fractional order and pseudo-second-order kinetic models showed satisfactory fit with the experimental data. The equilibrium data were well fitted by the Langmuir and Liu isotherm models, with a maximum sorption capacity of 104.2 mg/g. Also, the obtained values of thermodynamic parameters showed that the adsorption of MB onto AST is endothermic and spontaneous. The results of this study indicated that AST was a reliable adsorbent for removing cationic dyes from wastewater.

Keywords: Activated Spent Tea, Methylene Blue, Adsorption, Kinetic, Isotherm, Artificial Neural Network, Thermodynamic

INTRODUCTION

The rapid industrial growth has led to an increase of pollutant disposal into the environment. Industries such as textile, paper, plastic, pharmaceutical, rubber, cosmetics, leather and paint discharge noticeable amounts of colored wastewaters into the environment along with wastewater produced during the manufacturing process [1,2]. Dyes are organic compounds whose presence in effluents increase their chemical oxygen demand (COD) and decrease their biological degradability [3]. Reduced penetration of light in water and subsequent reduction of photosynthesis and oxygen are the other harmful effects of dyes [4]. Methylene blue (MB), a cationic dye, is the most commonly used dye for coloring cotton, wool and silk. MB is injurious to humans and animals: it tends to burn the eyes and cause methemoglobinemia, mental confusion, rapid or difficult breathing, nausea and vomiting [3,5].

Several technologies are available for decolorization of aqueous media, which are mainly put in three different categories: physical (exchange, membrane filtration), chemical (coagulation and flocculation) and biological [2]. The fact is that these techniques are often costly, lead to sludge production, and are efficient only in cases where the pollutant amounts are relatively high [6]. Adsorption, a physico-chemical treatment process, has been extensively applied as an effective method for treatment of dye-bearing wastewaters. Its main advantages include easy and low cost operation, simple design, insensitivity to toxic compounds, and effectiveness even at very low concentrations of contaminants [7].

In recent years, many researchers have used various adsorbents such as carbon nanotubes, graphite, anaerobic granular sludge, lignocellulosic, NaOH-modified rice husk, titanate nanotubes and sawdust for the removal of MB dye [5-11]. However, many of these adsorbents are expensive and difficult to prepare and regenerate, making it necessary to use low cost adsorbents. The waste materials and the by-products of agriculture and industrial activities could be used as low-cost adsorbents due to their abundance in nature and fewer processing requirements [1,2]. In this regard, spent tea is an industrial and household waste which can be used as an effective adsorbent. It is available in huge amounts worldwide, annually produced in Iran as much as about 1.05×10^8 kg. Spent tea is an oxygen demanding environmental contaminant that requires a long time for biodegradation. On the other hand, spent tea is an affordable absorbent because the saturated tea waste adsorbent can be incinerated and used as an adsorbent. Spent tea adsorbent has recently been used to remove heavy metals, dyes and organic com-

†To whom correspondence should be addressed.
E-mail: z.sharafabadi@yahoo.com

pounds [12-14].

In the present study, activated spent tea (labeled as AST) was prepared and used as an adsorbent for the removal of MB dye from aqueous solutions. Adsorption experiments were done in a batch system as a function of pH, contact time, adsorbent dosage, initial concentration of MB, and temperature. Then to determine the mechanism of the adsorption process, kinetic models were investigated. To evaluate and describe the experimental equilibrium data, nonlinear equilibrium isotherm models were used. Furthermore, artificial neural network (ANN) was employed to model and predict the effects of the operational parameters on the dye removal efficiency.

MATERIALS AND METHODS

1. Materials

MB (purity≥98.5%, empirical formula $C_{16}H_{18}ClN_3S{\cdot}3H_2O$; molecular weight 373.9 g/mol), (Merck, Germany) was used to prepare the stock solution. A stock solution with a concentration of 1,000 mg/L was prepared by dissolving 1 g of MB in deionized water. Concentrations of (10-100 mg/L) were then prepared by diluting the solution of stock with distilled water. Deionized water was used throughout all the experiments. All other chemicals were of analytical grade and were used without further purification.

2. Adsorbent Preparation and Characterization

Spent tea leaves were obtained from households. To completely remove impurities, the leaves were initially washed several times with deionized water. The sample was then boiled with deionized water at 100 °C for several times to remove the color. Decolorized spent tea leaves were dried at 65 °C for one day. Dried spent tea leaves were activated using sulfuric acid (H_2SO_4). To this aim, dried spent tea leaves were immersed in H_2SO_4 and were vigorously agitated for a few minutes followed by their washing in distilled water till the neutral pH of the filtrate was observed. The sulfuric acid was used to increase the proportion of active surfaces and prevent the elution of tannin compounds that would stain the treated water and increase the COD of solution. After drying at 105 °C, AST was crushed and eventually sieved through a range of sieves. Only particles between 250 and 100 µm diameter mesh sizes were used in accordance with the ASTM Method [15]. After sieving, AST particles were dried in an oven at 80-85 °C for 2 h and then stored in plastic bags until use.

Physicochemical features of the AST are listed in Table 1. The moisture and ash content of the adsorbent were measured using a digital microprocessor-based moisture analyzer (Mettler LP16) and ASTM D2866-11, respectively. CHNOS-Rapid Elemental Analytical Instrument (Elementer, Germany) was used for the elemental analysis of AST. The specific surface area of the AST measured by nitrogen adsorption/desorption apparatus (Quantachrome, 2000, NOVA) and Brunauer-Emmett-Teller (BET) model was found to be 285.5 m^2/g. The bulk density and particle size of adsorbent samples were determined using Gay-Lussac pycnometer and sieve analysis, respectively. The pH zero point of charge (pH_{pzc}) of the AST was determined accordingly with the procedure described by Cechinel et al. [16].

BRUKER's Vertex 70 infrared spectrometer was used for the Fourier transform infrared (FTIR) spectroscopy analysis. The surface morphologies of AST were obtained using a Philips XL-20 scanning electron microscope (SEM) (Philips Co., The Netherlands).

Table 1. Physicochemical features of AST

Parameters	Values
Moisture content (%)	3.72±0.4
Water soluble compounds (%)	1.2±0.3
Insoluble compounds (%)	95.1±0.4
Volatile fraction (%)	64.3±2.9
Ash content (%)	30.9±2.7
Elemental analysis (%)	
C	57.5±1.1
H	7.3±0.5
N	0.4
O	30.3±0.9
S	4.5±0.3
pH_{pzc}	5.0±0.2
Bulk density (kg/m^3)	258
Particle size (µm)	100-250
BET surface area (m^2/g)	285.5

3. Adsorption Experiments

In the present study, adsorbent efficiency for the removal of MB was evaluated through investigating various parameters. The experiment regarding the adsorption of MB onto AST was conducted by batch environment in 100 mL conical flasks containing 50 mL of solutions of MB and varying adsorbent dosages. The initial pH of solution was adjusted in the range of 2 to 10 by adding 0.1 M HCl and 0.1 M NaOH. The flasks were then shaken at a constant rate of 300 rpm for 5 h to reach the adsorption equilibrium conditions. The AST performance was also evaluated for the removal of MB from a simulated dye-house effluent. At appropriate time intervals, the aliquots were withdrawn from the solutions and centrifuged for 5 min at 5,000 rpm to separate AST particles. The residual MB concentrations in the supernatant solutions were determined by absorbance measurements using UV-visible spectrophotometer (Dr-5000, Hach Co.) at its maximum absorption wavelength of 668 nm. All the adsorption experiments were repeated in triplicates and the mean and the standard deviation (SD) of the values were used to compute the final results.

The removal efficiency (R) of MB and the adsorption capacity (q_e) was obtained using the following equations:

$$R(\%) = \frac{C_o - C_e}{C_o} \times 100 \quad (1)$$

$$q_e = \frac{C_o - C_e(V)}{m} \quad (2)$$

where q_e (mg/g) is the amount of MB adsorbed onto the unit amount of the adsorbent, C_o and C_e (mg/L) are the initial and equilibrium MB concentration, respectively, V (L) is the volume of the solution, and m (g) is the adsorbent mass in dry form.

After optimization of pH, the adsorption kinetics of MB onto AST was investigated with initial concentration of MB 100 mg/L at

different temperatures. The equilibrium isotherms were also investigated at initial concentrations of MB 50 mg/L at different temperatures using different adsorbent mass over a range of 0.1 to 20 g/L under optimal conditions obtained (optimum pH and contact time). The effect of the solution temperature on MB dye adsorption behavior was studied at 5, 25 and 50 °C and then the values of thermodynamic parameters were determined. Finally, simulated dye-house effluent containing different initial concentrations of MB were used in to verify the efficiency of AST as an adsorbent for the removal of dyes from textile effluents.

4. Mathematical Modeling Study

4-1. Adsorption Kinetic and Isotherm Models

The kinetic models were applied to understand the controlling mechanism of the adsorption process [17]. The data obtained from the adsorption of MB onto AST were analyzed using different kinetic models: pseudo-first order, pseudo-second order, Elovich, intraparticle diffusion, fractional power and the Avrami fractional order. The nonlinear equations and constants related to these kinetic models are given in Supplementary Table 1.

The equilibrium isotherms are necessary for designing the adsorption process as well as the description of the adsorption capacity for different contaminants. These can also give information about the surface characteristics of the adsorbent [6,14,17]. In this investigation, the adsorption isotherms were examined with Langmuir, Freundlich, Liu, Redlich-Peterson and Temkin models. The Langmuir isotherm model assumes that adsorption occurs homogeneously, while the Freundlich model assumes a heterogeneous adsorption of adsorbate onto the surface. The Redlich-Peterson isotherm model, on the other hand, describes adsorption on both homogeneous and heterogeneous surfaces. Therefore, this model has features of both the equilibrium models of Langmuir and Freundlich [18]. The parameters and non-linear equations of the adsorption isotherms are given in Supplementary Table 2. The fundamental characteristic of the Langmuir isotherm model was evaluated by the separation factor, R_L, to determine the favorability of the adsorption process. This factor indicates the shape of the isotherm to be one of unfavorable ($R_L>1$), favorable ($0<R_L<1$), irreversible ($R_L=0$) or linear adsorption ($R_L=1$). The values of R_L were calculated using the following equation:

$$R_L = \frac{1}{(1+K_L C_o)} \tag{3}$$

Table 2. Input and output variables and their ranges

Variable	Range
Input layer	
Dye concentration (mg/L)	10-100
Adsorbent dose (g/L)	0.1-20
pH	2-10
Temperature (K)	278-323
Time (min)	1-300
Output layer	
Dye removal efficiency (%)	14.2-99.99

4-2. Artificial Neural Network Model

Artificial neural network (ANN) is a technique used to model complex processes [19]. This technique, in which the processing units are neurons, has been used successfully to model water treatment processes [20]. ANN consists of three main layers of neurons called input, hidden and output layers. The layers, number of neurons (nodes) in each layer, and the transfer functions between layers form the network topology [21]. In this study, MB adsorption on AST was modeled by three-layered feed-forward back propagation neural network using linear transfer functions. A total of 81 experimental sets were used to feed the ANN structure. The data sets were divided into training, validation and test subsets that contained 61, 10, and 10 samples, respectively. The validation and test sets, for evaluation of the validation and modeling power of the nets, were randomly selected from the experimental data. The range of variables used in input and output layers is summarized in Table 2.

Training the ANN is sensitive to the number of neurons in the hidden layer. Therefore, a series of topologies in which the number of neurons in their hidden layer varied from 2 to 20 were used to model the adsorption process. Mean squared error (MSE) was applied to evaluate the effect of the number of neurons on modeling accuracy:

$$MSE = \left(\sum_{i=1}^{N} \left| (R_{i,\,pre} - R_{i,\,exp}) \right|^2 \right) / N \tag{4}$$

where N is the number of data point, $R_{i,pre}$ and $R_{i,exp}$ are network prediction and experimental dye removal efficiencies respectively, and i is an index of data.

Table 3. The FTIR spectral characteristics of AST before and after MB adsorption

IR peaks	Frequencies (cm^{-1})			Assignment	Ref.
	Before adsorption	After adsorption	Differences		
1	3397	3383	+14	Bonded -OH groups	[14,25]
2	2924	2924	0	Aliphatic C-H stretch	[26]
3	2853	2853	0	Aliphatic C-H stretch	[34]
4	1719	1719	0	Carbonyl stretch of carboxyl	[14]
5	1655	1655	0	C=O stretching	[35]
6	1519	1523	−4	Secondary amine group	[36]
7	1457	1451	+6	Symmetric bending of CH_3	[36]
8	1157	1160	−3	C=O stretching of ether groups	[37]

Table 4. Kinetic parameters for MB adsorption using AST adsorbent (Conditions: pH 7.0±0.1, adsorbent mass 10 g/L, C_o=100 mg/L)

Adsorption kinetic models	Parameters	Temperature (K)		
		278	298	323
	$q_{e,exp}$ (mg/g)	**8.6**	**9.5**	**10**
Pseudo-first order $q_t=q_e\,(1-\exp(-k_f t))$	q_e (mg/g)	8.606	9.207	9.73
	k_f (min^{-1})	0.05	0.1557	0.39
	RMSE	0.65	0.8161	0.544
	SSE	4.644	7.326	3.252
	R^2adj	0.961	0.935	0.97
Pseudo-second order $q_t=\frac{k_s q_e^2 t}{1+q_e k_s t}$	k_S (g/mg·min)	0.0072	0.0256	0.060
	q_e (mg/g)	9.485	9.702	10.14
	RMSE	0.4121	0.3819	0.205
	SSE	1.868	1.604	0.464
	R^2adj	0.984	0.986	0.996
Avrami fractional order $q_t=q_e\{1-\exp[-(k_{AV}t)]^{nAV}\}$	k_{AV} (min^{-1})	0.036	0.1164	0.3370
	q_e (mg/g)	9.33	9.738	9.993
	n_{AV}	0.60	0.517	0.588
	RMSE	0.199	0.164	0.142
	SSE	0.397	0.270	0.201
	R^2adj	0.996	0.997	0.998
Power fraction $q_t=at^b$	a (mg/g·min^b)	2.144	4.086	6.034
	b	0.2724	0.1696	0.104
	RMSE	0.709	0.8378	1.005
	SSE	5.529	7.721	11.11
	R^2adj	0.953	0.9314	0.895
Elovich $q_t=\left(\frac{1}{\beta}\right)\ln(1+\alpha\beta t)$	α (mg/g·min)	1.722	14.93	312.3
	β (g/mg)	0.589	0.772	1.051
	RMSE	0.394	0.546	0.863
	SSE	1.746	3.278	8.19
	R^2adj	0.985	0.97	0.922
Intraparticle diffusion $q_t=k_{id}t^{0.5}+C$	k_{id} (mol/g·$min^{0.5}$)	0.526	0.46	0.371
	C	1.801	3.727	5.434
	RMSE	1.237	1.823	2.308
	SSE	16.83	36.57	58.6
	R^2adj	0.86	0.68	0.44

5. Models Fitness

In the present study, the parameters of kinetic and isotherm models were determined based on the non-linear method by using the MATLAB® 7.11.0 (R2010b) with the Levenberg-Marquardt algorithm. To select the most suitable kinetic and isotherm model, it is necessary to evaluate their validity. Here, the validity of kinetic and isotherm models was assessed by criteria such as the adjusted determination factor (R^2adj), the sum of squared error (SSE) and the root mean square error (RMSE). These criteria describe the goodness of fit between the experimental and predicted data. R^2adj, SSE and RMSE can be calculated according to Supplementary Table 3.

6. Simulated Dye-house Effluent

To imitate the effluent produced by typical textile industries using reactive dyes, a simulated dye-house effluent containing five typical dyes commonly used as fabric colorants together with auxiliary chemicals was prepared at pH 7.0. Typically, between 10-60% of synthetic dyes and almost the entire dye bath auxiliaries remain in the spent dye bath and its composition is diluted 5- to 30-fold during the next regular washing and rinsing steps [22-23]. The characteristics of the simulated dye-house effluent are summarized in Supplementary Table 4.

RESULTS AND DISCUSSION

1. Characterizations of AST

Fig. 1 shows the electron micrographs for the spent tea and AST. Clearly, the AST surface is different from that of the spent tea. As Fig. 1 shows, the AST has an irregular and a more porous structure than spent tea. This is associated with the removal of impurities from the spent tea during the acid activation process. Therefore,

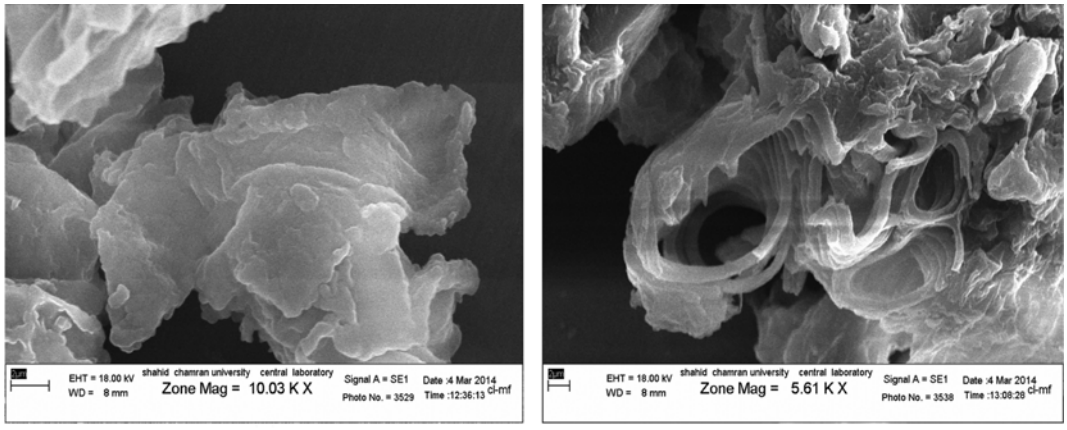

Fig. 1. SEM micrograph (a) spent tea (b) AST.

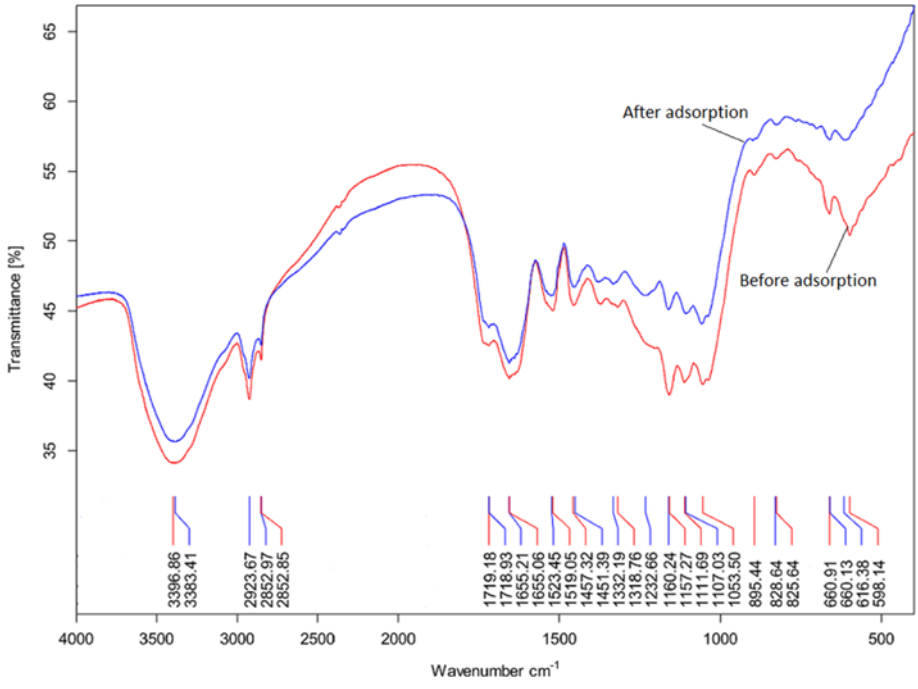

Fig. 2. FTIR spectra of AST before and after MB adsorption.

acid activation has increased both the porosity and the active surface of AST. This finding can be confirmed by the high specific surface area of AST (285.5 m^2/g) than raw spent tea (21 m^2/g) [24].

Fig. 2 shows the FTIR spectrum of the AST before and after the MB was loaded. The FTIR spectroscopic characteristics are shown in Table 3. The bands around 3,400 cm^{-1} indicated the presence of bonded -OH groups [14,25]. The bands observed at about 2,920-2,850 cm^{-1} could be assigned to the aliphatic C-H group [26]. As shown in Fig. 2 and Table 3, the spectra display a number of absorption peaks, indicating the complex nature of the AST. As seen in Table 3, the spectral analysis before and after MB adsorption indicated only slight changes in the bonded -OH groups, secondary amine group, C=O stretching of ether group and symmetric bending of CH_3 of the AST showing that the adsorption process may be physicochemical in nature.

2. Effect of pH

The pH of solution plays a key role in the adsorption process. It can also affect the solution chemistry, adsorbent surface charge, and the functional groups on the active sites. Referring to Fig. 3, dye adsorption percentages increased by an increase of pH from 2 to 10 for 50 mg/L concentrations of MB. Low adsorption at pH below 5 can be attributed to the electrostatic repulsion between the adsorbent and the adsorbate. When the solution pH is lower than pH_{pzc} ($pH<pH_{pzc}$), the surface of the adsorbent is positive, leading to an electrostatic repulsion between MB cations and AST, which results in a decrease in the adsorption percentage. Moreover, in acidic pH, the H^+ ions exist at high concentrations, which compete with MB cations for active sites onto the AST. This result is in good agree-

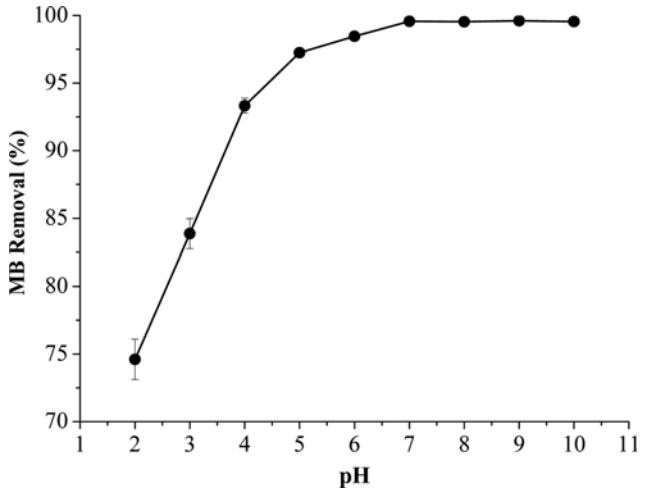

Fig. 3. The effect of pH on the MB dye adsorption by AST (Conditions: contact time 60 min, adsorbent dose 5.0 g/L, 298 K).

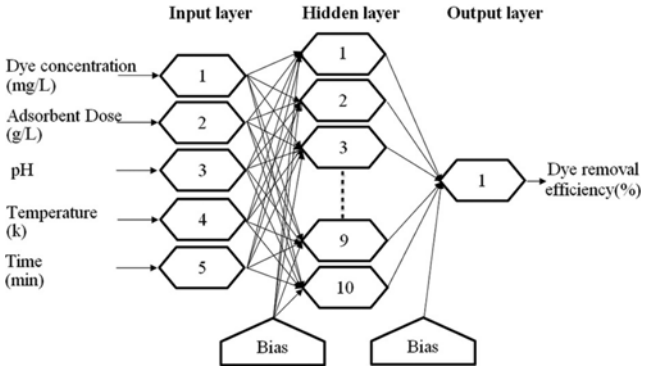

Fig. 4. The ANN optimized structure.

ment with the previous studies for MB adsorption on different adsorbents [14]. In contrast, at pH>pH_{pzc}, the adsorbent surface becomes negatively charged due to the presence of hydroxide ions (OH^-) and, consequently, the MB cations are easily adsorbed onto it by electrostatic attraction forces. The value of pH of the AST at the point of zero charge was found to be 5.0±0.2 according to Table 1. Thus pH values greater than 5.0 will be favorable conditions for MB adsorption on the AST. Therefore, based on the fact that most sewage and water pH ranges at about neutral (6.0-8.0), the optimum pH 7.0 was selected throughout the study.

3. ANN Modeling

The optimum ANN with input, hidden and output layers of 5, 10 and 1, respectively, was used to model the adsorption process (Fig. 4). The weights and biases of optimized ANN topology used in this study are listed in Supplementary Table 5.

The agreement between the predicted ANN model and the experimental values of dye removal efficiency for the test sets is shown in Fig. 5. The plot in this figure has a correlation coefficient of 0.999 for the test set. These results confirmed that the neural network model is a good way of predicting the experimental data within the adopted ranges.

The relative importance of input variables on the value of dye

Table 5. Isotherm constants of different models for the adsorption of MB onto AST (Conditions: pH 7.0±0.1, contact time 120 min, adsorbent mass 0.1-20 g/L, C_o=50 mg/L)

Adsorption isotherm models	Parameters	Temperature (K)		
		278	298	323
Langmuir				
$q_e=\frac{K_L q_m C_e}{1+K_L C_e}$	q_m (mg/g)	41.1	55.08	104.2
	K_L (L/mg)	0.04	0.036	0.031
	R_L	0.2	0.22	0.24
	R^2adj	0.996	0.994	0.992
	RMSE	0.703	1.104	2.039
	SSE	4.448	10.97	37.42
Freundlich				
$q_e=K_F C_e^{1/n}$	K_F (L/g)	2.888	3.638	5.614
	n	1.702	1.684	1.574
	R^2adj	0.99	0.991	0.984
	RMSE	1.102	1.35	2.986
	SSE	10.93	16.41	80.24
Redlich-Peterson				
$q_e=\frac{K_{RP} C_e}{1+a_{RP} C_e^g}$	K_{RP} (L/g)	1.482	1.756	2.43
	a_{RP} (L/mg)	0.02	0.015	0.0003
	g (-)	1.143	1.187	2.096
	R^2adj	0.996	0.993	0.996
	RMSE	0.7315	1.159	1.438
	SSE	4.28	10.74	16.54
Liu				
$q_e=\frac{q_m (K_g C_e)^n}{1+(K_g C_e)^n}$	K_g (L/mg)	0.034	0.043	0.058
	n	0.8734	0.9469	1.361
	q_m (mg/g)	44.01	67.32	75.84
	R^2adj	0.996	0.994	0.994
	RMSE	0.7383	1.13	1.847
	SSE	4.361	10.24	27.29
Temkin				
$q_e=B\ln(A_T C_e)$	A_T (L/g)	3.673	9.126	35.38
$B=\frac{RT}{b_T}$	B	4.459	4.537	5.723
	R^2adj	0.8476	0.767	0.659
	RMSE	4.295	6.751	13.68
	SSE	166	410.2	1684

removal efficiency (%) was calculated by Eq. (5)

$$I_j=\frac{\sum_{m=1}^{m=N_h}\left(\left(\left|W_{jm}^{ih}\right|/\sum_{k=1}^{k=N_i}\left|W_{km}^{ih}\right|\right)\times\left|W_{mn}^{ho}\right|\right)}{\sum_{k=1}^{k=N_i}\left\{\sum_{m=1}^{m=N_h}\left(\left(\left|W_{jm}^{ih}\right|/\sum_{k=1}^{N_i}\left|W_{km}^{ih}\right|\right)\times\left|W_{mn}^{ho}\right|\right)\right\}} \quad (5)$$

where I_j is the relative importance of the j_{th} input variable on the output variable, Ws are connection weights, N_i and N_h are the numbers of input and hidden neurons; the superscripts 'i', 'h' and 'o' refer to input, hidden and output layers; and subscripts 'k', 'm' and 'n' refer to input, hidden and output neurons [21]. According to the obtained results, the relative importance of dye concentration, adsorbent dose, pH, Temperature, and Time on dye removal efficiency

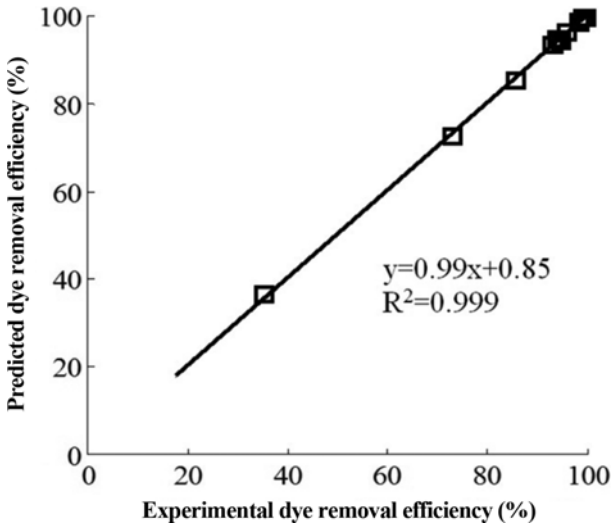

Fig. 5. Simulated results vs. experimental results for dye removal efficiency.

was 14.10, 30.03, 10.96, 9.47 and 35.44%, respectively.

4. Adsorption Kinetics

The effect of contact time on the removal of MB dye by AST was studied at a period of 0-300 minutes, the optimum pH of 7.0 and the adsorbent dosage of 10 g/L at 278-323 K for 100 mg/L concentrations of MB (see Fig. 6). Note that the adsorption capacity rate of dye was fast during the early adsorption stage of contact time. This phenomenon can be explained by the fact that active sites are initially vacant and then filled by increasing the contact time. It is observed from Fig. 6 that the adsorption capacity of MB was almost constant for the contact times after 120 minutes. In fact, the adsorption process reaches the equilibrium point at 120 min. Therefore, this was chosen as the equilibrium time of MB adsorption onto AST.

To describe the adsorption kinetics of MB using AST, six kinetic models were tested, as shown in Fig. 6. Taking into account that the RMSE and SSE values obtained by pseudo-first order (PFO), Power fraction (P-F), Elovich and Intraparticle diffusion (I-D) kinetic models were greater than the values obtained with the Avrami fractional and pseudo-second order (PSO) models, it can thus be concluded that the adsorption of MB on AST follows the Avrami fractional model and the pseudo-second order model. The Avrami and pseudo-second order kinetic parameters of MB adsorption on AST are listed in Table 4. Moreover, the calculated equilibrium adsorption capacity, $q_{e,cab}$ using Avarmi and pseudo-second order models are very close to the experimental $q_{e,exp}$ values (Table 4). Liu et al. and Zhao and Liu showed that the pseudo-second order model provides a better fitting to the experimental data for the MB adsorption onto graphite powder and anaerobic granular sludge, respectively [7,11].

Table 4 shows that the rate coefficients for Avrami and second-order kinetic models (k_{AV} and k_s) increased with increasing solution temperature. It was understood that with the increase of temperature, the adsorption rate constants enhanced. These findings imply that the adsorption of MB on AST is more favorable at higher temperatures. As observed in Table 4, the values of C of interaparticle diffusion model are not equal to zero at all studied temperatures, indicating that intraparticle diffusion is not the only controlling step for MB adsorption process. Therefore, the rate-limiting step

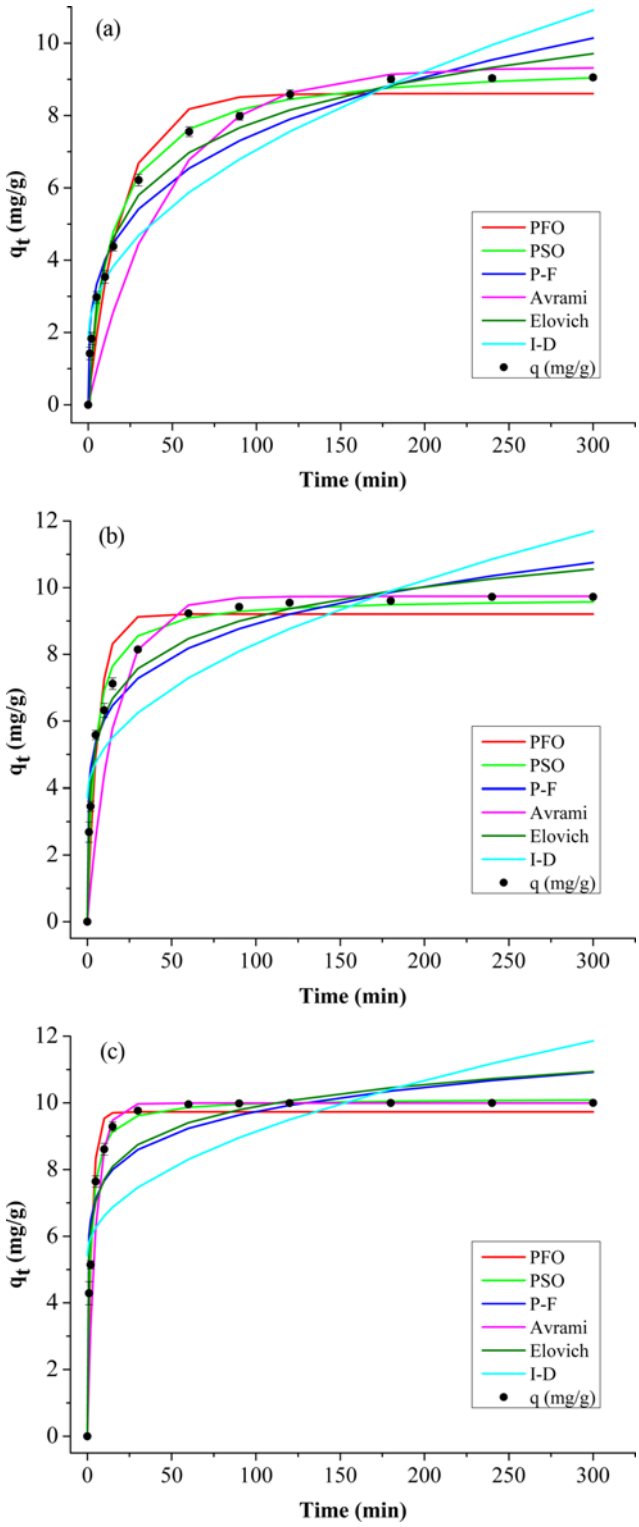

Fig. 6. Non-linear adsorption kinetics of MB on AST adsorbent: (a) 278 K; (b) 298 K; (c) 323 K; (Conditions: pH 7.0±0.1, adsorbent mass 10 g/L, $C_{o,MB}$ 100 mg/L).

maybe is a complex combination of the boundary layer and intra-particle diffusion [27].

5. Adsorption Isotherms

For the equilibrium study, the contact time was 2 h for MB adsorption to obtain the state of equilibrium at optimum pH 7.0. The effect of temperature on MB adsorption is shown in Table 5. The results revealed that the sorption capacity for initial dye concentration of 50 mg/L increased from 41.1 to 104.2 mg/g with the temperatures increasing from 5 to 50 °C. This behavior revealed that the MB adsorption onto AST is endothermic. The effect of temperature is fairly common and increases the mobility of the dye cations. Furthermore, an increase in temperature may cause the swelling effect within the internal structure of the AST adsorbent, enabling more penetration of MB molecules into the adsorbent pores. The increase of the adsorption yield and adsorption capacity at increased temperatures indicated that the adsorption of MB dye by AST may involve not only physical but also chemical sorption. This can be due to an increase in bond rupture, and consequently an increase in active sites at high temperatures [28].

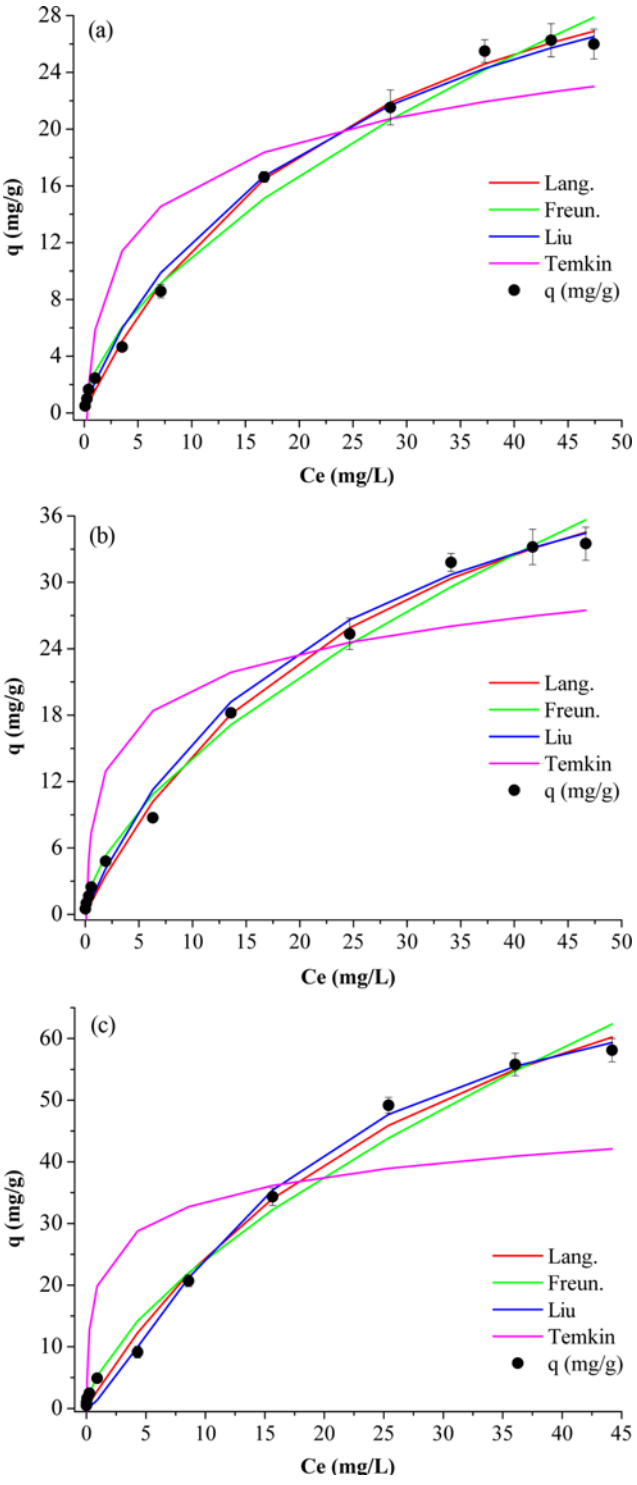

Fig. 7. The plots of non-linear models of isotherms for MB adsorption onto AST: (a) 278 K; (b) 298 K; (c) 323 K; (Conditions: pH 7.0±0.1, contact time 120 min, $C_{o,MB}$ 50 mg/L).

Analysis of the equilibrium data is important in designing adsorption systems. In this study, the Langmuir, Freunlich, Liu, Redlich-Peterson (R-P) and Temkin models were tested using non-linear equations. Parameters of the adsorption equilibrium isotherms of MB onto AST were obtained at various MB concentrations and temperatures given in Table 5.

Despite the fact that the Redlich-Peterson (R-P) model was the best isotherm model for MB adsorption by AST adsorbent based on the R^2adj, RMSE and SSE, since g is more than 1, this isotherm model is invalid. Regardless of the Redlich-Peterson (R-P) model, the Langmuir and Liu models showed the lowest RMSE and SSE values (Table 5). Additionally, the best fit is obtained through combining the Langmuir and Liu models by employing a nonlinear method (see Fig. 7). The Langmuir model suggests a uniform distribution of homogeneous active sites on the adsorbent surface as well as a monolayer and homogeneous adsorption of MB on the AST [22]. Moreover, as shown in Table 5, it is obvious that the obtained values of R_L dimensionless separation factor are less than one in all the studied temperatures, confirming favorable adsorption of MB onto AST. Previous studies have also reported that the

Table 6. Comparison of maximum adsorption capacity of several biosorbents for MB adsorption at the best experimental conditions of each work

Adsorbent	q_{max} (mg/g)	R^2	Reference
Tea waste	85.16	Not reported	[14]
Date palm leaves	58.1	0.912	[38]
Cocoa pod husk	263.9	0.952	[39]
Acacia fumosa seed shell	10.5	0.9104	[40]
Albizia lebbeck seed pods	328.3	0.9871	[41]
Pistacia khinjuk	185.18	0.9973	[42]
Gralic peel	142.86	0.97	[43]
Modified sawdust	111.5	0.974	[44]
Modified pine sawdust	93.5	0.993	[45]
Raw pine cone	129.9	0.996	[46]
Modified pine cone	142.9	0.99	[46]
Rice husk	28.5	0.999	[47]
Modified loofah	85.5	0.941	[48]
Activated spent tea (AST)	104.2	0.992	This study

Langmuir isotherm was the best model for the experimental data of MB adsorption on other adsorbents as well [6,10,11,14]. Table 6 presents a comparison of sorption capacities of MB adsorbed in different low-cost agro-waste based adsorbents. The maximum amount of MB uptake per unit mass of AST was 104.2 mg/g based on the Langmuir equilibrium model. According to Table 6, the AST adsorbent presented good sorption capacities compared with other adsorbents.

6. Adsorption Thermodynamic

The thermodynamic parameters including the Arrhenius activation energy (Ea), entropy change (ΔS^o), enthalpy change (ΔH^o) and Gibbs free energy change (ΔG^o) were obtained using the following equations [11]:

$$\ln k_{AV} = \ln k_o - \frac{Ea}{RT} \quad (6)$$

$$\Delta G^o = -RT\ln(K_L) \quad (7)$$

$$\ln(K_L) = \frac{\Delta S^o}{R} - \frac{\Delta H^o}{RT} \quad (8)$$

where k_o is the Arrhenius factor, R is the gas constant (8.3145 J/mol K), and K_L is the Langmuir equilibrium constant (*l*/mol) at temperature T.

The magnitude of the activation energy is commonly used as the basis for differentiating between physical and chemical adsorption. The activation energy for physisorption usually ranges from 5 to 40 kJ/mol since the forces involved in physisorption are weak. Whereas, chemisorption as a chemical process requires more energy and generally has activation energies above 40 kJ/mol [29,30]. A linear plot of ln k_{AV} versus 1/T for the adsorption of MB onto the AST was constructed to determine the Ea value from the slope using the Arrhenius equation (figure not shown). The activation energy was calculated to be 37.06 kJ/mol at pH 7.0±0.1 with a linear regression coefficient of 0.997. The value is of the same magnitude as the activation energy of physisorption. The positive values of Ea suggested that increasing the temperature favored the adsorption and adsorption process may be an endothermic in nature.

Considering the relationship between ΔG^o and K_L, ΔS^o and ΔH^o were determined from the slope and intercept of the van't Hoff plots of ln(K_L) versus 1/T (R^2=0.990). The values of ΔH^o and ΔS^o are both positive and found to be 8.9 kJ/mol and 110.4 J/mol K, respectively. The positive values of ΔH^o demonstrate that the adsorption process has been endothermic. Kara et al. [31] suggested that the ΔH^o of physisorption is smaller than 40 kJ/mol. Based on ΔH^o, this study suggested that the adsorption of MB onto AST was a physisorption process. The positive value of ΔS^o indicates the tendency of AST for MB and suggests some structural changes in dye and AST. Furthermore, the positive values of ΔS^o show an increasing randomness at the AST-solution and an adsorption medium interface during the adsorption. The values of ΔG^o were obtained (−21.8), (−23.9) and (−26.8) kJ/mol for 278, 298 and 323 K, respectively. The negative value of ΔG^o indicates the spontaneous nature of MB adsorption onto AST. The values of ΔG^o have decreased as a result of increasing the temperature, indicating that the adsorption of MB onto AST is more favorable at higher temperatures [6,32]. These results are also in good agreement with the previous reports for MB adsorption on different adsorbents [6,33].

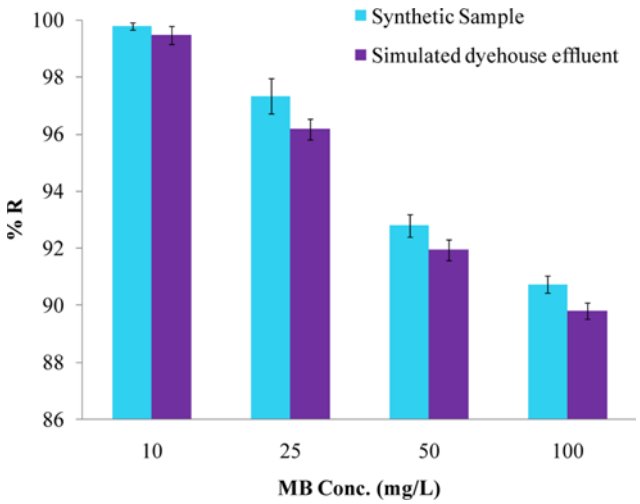

Fig. 8. The comparison the removal of MB by AST in synthetic and real samples (Conditions: pH 7.0±0.1, adsorbent mass 10.0 g/L, contact time 30 min, 298 K).

7. Treatment of a Simulated Dye-house Effluent

To evaluate application of AST for treatment of industrial textile effluents, simulated dye-house effluents containing 10-100 mg/L of MB were utilized (see Supplementary Table 4). According to Fig. 8, almost no noticeable difference was observed in the adsorption yields between the synthetic and simulated dye-house effluents at all initial MB concentrations. This result suggests that AST enjoys a good potential for the removal of dye in real samples. Therefore, the removal of MB dye from industrial wastewaters using AST as a low-cost adsorbent can be a cost-effective and useful method.

CONCLUSION

Spent tea, an industrial and household waste, was activated and used as an effective bio-sorbent to remove MB dye from aqueous solutions. The initial pH was found to significantly influence the MB uptake, and the maximum adsorption of MB on AST was at natural basic pH. The equilibrium data were best described by the Langmuir and Liu isotherm models, with the results suggesting that the adsorption capacity increased as a result of increasing temperature. The maximum adsorption capacity was 104.2 mg/g at pH 7.0±0.1. Adsorption data were modeled by using six different kinetic models, among which the Avrami fractional order and the pseudo-second order kinetic models could best describe the sorption kinetics. The mathematical model developed using ANN could precisely predict the effect of dye concentration, adsorbent dose, pH, time and temperature on adsorption efficiency with a satisfactory correlation coefficient of 0.999. The adsorbent dose and time, with a relative importance of 30.03 and 35.44% respectively, appeared to be the most influential parameters in the MB adsorption. Changes in the standard Gibbs free energy (ΔG^o), standard enthalpy (ΔH^o) and standard entropy (ΔS^o) showed that the adsorption of MB dye onto AST was spontaneous and endothermic. This study shows that AST is a promising bio-sorbent for the removal of dye from colored wastewaters.

ACKNOWLEDGEMENT

The authors would like to thank the Student Research Committee and the Research and Technology Deputy of Ahvaz Jundishapur University of Medical Sciences for financial support (grant No: 92.S.12).

REFERENCES

1. M. K. P. Reddy, S. Mahammadunnisa, B. Ramaraju, B. Sreedhar and C. Subrahmanyam, *Environ. Sci. Pollut. Res.*, **20**, 4111 (2013).
2. M. Rafatullah, O. Sulaiman, R. Hashim and A. Ahmad, *J. Hazard. Mater.*, **177**, 70 (2010).
3. A. S. Franca, L. S. Oliveira and M. E. Ferreira, *Desalination*, **249**, 267 (2009).
4. L. S. Oliveira, A. S. Franca, T. M. Alves and S. D. Rocha, *J. Hazard. Mater.*, **155**, 507 (2008).
5. S. Chowdhury and P. Saha, *Environ. Sci. Pollut. Res.*, **20**, 1050 (2013).
6. Y. Yao, F. Xu, M. Chen, Z. Xu and Z. Zhu, *Bioresour. Technol.*, **101**, 3040 (2010).
7. F. Liu, S. Teng, R. Song and S. Wang, *Desalination*, **263**, 11 (2010).
8. A. Ahmad, M. Rafatullah, O. Sulaiman, M. Ibrahim and R. Hashim, *J. Hazard. Mater.*, **170**, 357 (2009).
9. L. W. Low, T. T. Teng, M. Rafatullah, N. Morad and B. Azahari, *Sep. Sci. Technol.*, **48**, 1688 (2013).
10. L. Xiong, Y. Yang, J. Mai, W. Sun, C. Zhang, D. Wei, Q. Chen and J. Ni, *Chem. Eng. J.*, **156**, 313 (2010).
11. M. Zhao and P. Liu, *Desalination*, **249**, 331 (2009).
12. F. Bolat, A. Govori, A. Haziri, S. Spahiu and F. Faiku, *J. Int. Environ. Appl. Sci.*, **5**, 63 (2010).
13. E. Malkoc and Y. Nuhoglu, *Sep. Purif. Technol.*, **54**, 291 (2007).
14. M. T. Uddin, M. A. Islam, S. Mahmud and M. Rukanuzzaman, *J. Hazard. Mater.*, **164**, 53 (2009).
15. American Society for Testing and Material (ASTM), *Annual book of astm, standard test method for performing the sieve analysis of coal and designating coal size, method d4749*, USA (2012).
16. M. A. P. Cechinel, S. M. A. G. Ulson de Souza and A. A. Ulson de Souza, *J. Clean. Prod.*, **65**, 342 (2013).
17. A. A. Babaei, Z. Baboli, N. Jaafarzadeh, G. Goudarzi, M. Bahrami and M. Ahmadi, *Desalination and Water Treatment*, **53**, 768 (2015).
18. A. Behnamfard and M. M. Salarirad, *J. Hazard. Mater.*, **170**, 127 (2009).
19. N. G. Turan, B. Mesci and O. Ozgonenel, *Chem. Eng. J.*, **171**, 1091 (2011).
20. S. Dutta, S. A. Parsons, C. Bhattacharjee, S. Bandhyopadhyay and S. Datta, *Expert. Systems with Appl.*, **37**, 8634 (2010).
21. A. R. Khataee, G. Dehghan, A. Ebadi, M. Zarei and M. Pourhassan, *Bioresour. Technol.*, **101**, 2252 (2010).
22. L. D. T. Prola, E. Acayanka, E. C. Lima, C. S. Umpierres, J. C. P. Vaghetti, W. O. Santos, S. Laminsi and P. T. Djifon, *Industrial Crops and Products*, **46**, 328 (2013).
23. M. C. Ribas, M. A. Adebayo, L. D. T. Prola, E. C. Lima, R. Cataluña, L. A. Feris, M. J. Puchana-Rosero, F. M. Machado, F. A. Pavan and T. Calvete, *Chem. Eng. J.*, **248**, 315 (2014).
24. A. Ebrahimian, E. Saberikhah, M. S. Emami and M. Badrouh, *Cellulose Chem. Technol.*, **48**, 735 (2014).
25. A. A. Oladipo, M. Gazi and S. Saber-Samandari, *J. Taiwan Institute Chem. Engineers*, **45**, 653 (2014).
26. A. A. Oladipo and M. Gazi, *J. Water Process Eng.*, **2**, 43 (2014).
27. B. Kakavandi, A. Esrafili, A. Mohseni-Bandpi, J. A. Jonidi and K. R. Rezaei, *Water science and technology: a J. of the International Association on Water Pollution Research*, **69**, 147 (2014).
28. E. Malkoc and Y. Nuhoglu, *J. Hazard. Mater.*, **127**, 120 (2005).
29. H. K. Boparai, M. Joseph and D. M. O'Carroll, *J. Hazard. Mater.*, **186**, 458 (2011).
30. Y. Cantu, A. Remes, A. Reyna, D. Martinez, J. Villarreal, H. Ramos, S. Trevino, C. Tamez, A. Martinez, T. Eubanks and J. G. Parsons, *Chem. Eng. J.*, **254**, 374 (2014).
31. M. Kara, H. Yuzer, E. Sabah and M. S. Celik, *Water Res.*, **37**, 224 (2003).
32. M. Greluk and Z. Hubicki, *Chem. Eng. J.*, **162**, 919 (2010).
33. C.-H. Weng and Y.-F. Pan, *J. Hazard. Mater.*, **144**, 355 (2007).
34. Y.-S. Yun, D. Park, J. M. Park and B. Volesky, *Environ. Sci. Technol.*, **35**, 4353 (2001).
35. A. Kapoor and T. Viraraghavan, *Bioreso. Technol.*, **61**, 221 (1997).
36. E. Malkoc and Y. Nuhoglu, *J. Hazard. Mater.*, **135**, 328 (2006).
37. E. Malkoc and Y. Nuhoglu, *Chem. Eng. Sci.*, **61**, 4363 (2006).
38. M. Gouamid, M. R. Ouahrani and M. B. Bensaci, *Energy Procedia*, **36**, 898 (2013).
39. F. l. Pua, M. S. Sajab, C. H. Chia, S. Zakaria, J. A. Rahman and M. S. Salit, *J. Environ. Chem. Eng.*, **1**, 460 (2013).
40. M. Kumar and R. Tamilarasan, *J. Environ. Chem. Eng.*, **1**, 1108 (2013).
41. M. J. Ahmed and S. K. Theydan, *J. Anal. Appl. Pyrol.*, **105**, 199 (2014).
42. M. Ghaedi, A. M. Ghaedi, F. Abdi, M. Roosta, A. Vafaei and A. Asghari, *Ecotoxicol. Environ. Saf.*, **96**, 110 (2013).
43. B. Hameed and A. Ahmad, *J. Hazard. Mater.*, **164**, 870 (2009).
44. W. Zou, H. Bai, S. Gao and K. Li, *Korean J. Chem. Eng.*, **30**, 111 (2013).
45. R. Zhang, Y. Zhou, X. Gu and J. Lu, *CLEAN - Soil, Air, Water*, **43**, 96 (2015).
46. M. Yagub, T. Sen and M. Ang, *Environ. Earth Sci.*, **71**, 1507 (2014).
47. M. K. P. Reddy, K. Krushnamurty, S. K. Mahammadunnisa, A. Dayamani and C. Subrahmanyam, *Int. J. Environ. Sci. Technol.*, **12**, 1363 (2015).
48. J. X. Yu, L. Y. Wang, R. A. Chi, Y. F. Zhang, Z. G. Xu and J. Guo, *Res. Chem. Intermed*, **39**, 3775 (2013).

Supporting Information

Optimization of cationic dye adsorption on activated spent tea: Equilibrium, kinetics, thermodynamic and artificial neural network modeling

Ali Akbar Babaei[*,], Alireza Khataee[***], Elham Ahmadpour[****], Mohsen Sheydaei[***], Babak Kakavandi[**], and Zahra Alaee[*****,†]**

[*]Environmental Technologies Research Center, Ahvaz Jundishapur University of Medical Sciences, Ahvaz, Iran
[**]Department of Environmental Health Engineering, School of Public Health, Ahvaz Jundishapur University of Medical Sciences, Ahvaz, Iran
[***]Research Laboratory of Advanced Water and Wastewater Treatment Processes, Department of Applied Chemistry, Faculty of Chemistry, University of Tabriz, Tabriz, Iran
[****]Department of Health, Ahvaz Jundishapur University of Medical Sciences, Ahvaz, Iran
[*****]Student Research Committee, Ahvaz Jundishapur University of Medical Sciences, Ahvaz, Iran
(*Received 30 June 2014 • accepted 13 November 2014*)

Suppl. Table 1. Mathematical equations of the used kinetic adsorption models

Model	Equation	Parameter and dimension
Pseudo-first order (Lagergern)	$q_t=q_e(1-\exp(-k_f t))$	K_f (min^{-1}) q_e, q_t (mg g^{-1})
Pseudo-second order (Ho)	$q_t=\frac{k_s q_e^2 t}{1+q_e k_s t}$	k_S (min^{-1}) t: time (min)
Elovich	$q_t=\left(\frac{1}{\beta}\right)\ln(1+\alpha\beta t)$	α (mg g^{-1} min^{-1}) β (g mg^{-1})
Avrami fractional order	$q_t=q_e\{1-\exp[-(k_{AV}t)]^{nAV}\}$	k_{AV} (min^{-1}) n_{AV} (–)
Intraparticle diffusion	$q_t=k_{id}t^{1/2}+C$	k_{id} (mg g^{-1} $min^{-0.5}$) C (–)
Fractional power	$q_t=at^b$	a (mg g^{-1} min^{-b}), b (–)

NOTE: Parameters k_f (1/min) and k_S (mg/g·min) are rate coefficient for pseudo-first and pseudo-second order kinetic models, respectively. α is the initial adsorption rate (mg/g·min), β is the adsorption constant (g mg^{-1}). k_{id} (mg g^{-1} $min^{-0.5}$) is the constant rate of intra-particle diffusion, and C is the constant depicting the boundary layer effects. a (mg g^{-1} min^{-b}) and b are the fractional power kinetic model constants, k_{AV} and n_{AV} are the Avrami rate constant (min^{-1}) and fractional reaction order (Avrami), respectively. q_e and q_t (mg/g) are adsorption capacity at equilibrium and at time t, respectively

Suppl. Table 2. Mathematical equations of the used isotherm adsorption models

Model	Equation	Parameter and dimension
Langmuir	$q_e=\frac{K_L q_m C_e}{1+K_L C_e}$	q_m (mg g^{-1}) K_L (L mg^{-1})
Freundlich	$q_e=K_F C_e^{1/n}$	K_F (mg g^{-1})(mg L^{-1})$^{-n}$ n: model exponent (−)
Redlich-Peterson	$q_e=\frac{K_{RP} C_e}{1+a_{RP} C_e^g}$	K_{RP} (L g^{-1}) a_{RP} (L mg^{-1}) g (−) (0<g<1)
Temkin	$q_e=B\ln(A_T C_e)$ $B=\frac{RT}{b_T}$	B (J mol^{-1}) A_T (L g^{-1}) b_T (−)
Liu	$q_e=\frac{q_m (K_g C_e)^n}{1+(K_g C_e)^n}$	K_a (L mg^{-1}) n (−) (0<n<1)

NOTE: q_o is the maximum adsorption capacity (mg g^{-1}) and k_L is the adsorption equilibrium constant (L mg^{-1}), K_F and n are the adsorption capacity and the adsorption intensity, respectively. K_g (L mg^{-1}) and n_L are the constants related to Liu isotherm model. A_{RP}, B_{RP} and g are Redlich-Peterson constants, which values of g lies between 0 and 1. For g=1, R-P equation convert to Langmuir form. When A_{RP} and B_{RP} are much greater than unity, the equation can transform Freundlich form. B is Constant related to heat of sorption (J mol^{-1}), A_T is Temkin isotherm equilibrium binding constant (L g^{-1}), b_T is Temkin isotherm constant, R=universal gas constant (8.314 J/mol/K) and T=temperature at 298 K

Suppl. Table 3. Lists of the coefficients of determination and error functions

Goodness of fit criteria	Abbreviation	Definition/expression
Adjusted determination factor	R^2adj	$R^2_{adj}=\left\{1-\left[1-\left(\frac{\sum_i^n (q_{i,exp}-q_{i,exp})^2-\sum_i^n (q_{i,exp}-q_{i,calc})^2}{\sum_i^n (q_{i,exp}-q_{i,exp})^2}\right)\cdot\left(\frac{n-1}{n-p}\right)\right]\right\}$
Sum squared error	SSE	$SSE=\sum_{i=1}^n (q_{i,calc}-q_{i,exp})_i^2$
Root mean square error	RMSE	$RMSE=\sqrt{\frac{\sum_{i=1}^n (q_{i,exp}-q_{i,exp})_i^2}{n}}$

Where $q_{i,calc}$ is each value of q predicted by the fitted model, $q_{i,exp}$ is each value of q measured experimentally, $\overline{q}_{i,exp}$ is the average of q measured experimentally, n is the number of experiments performed and p is the number of parameters of the fitted model. The best model is the model with the lowest RMSE and SSE, as well as with R^2adj with R^2 close to one

Suppl. Table 4. Characteristics and composition of the simulated dye-house effluent

	Concentration (mg L^{-1})
Dyes	
Methylene blue (λ_{max} 668 nm)	10-100
Reactive orange 16 (λ_{max} 489 nm)	5.0
Reactive black 5 (λ_{max} 598 nm)	5.0
Cibacron brilliant yellow 3G-P (λ_{max} 402 nm)	5.0
Reactive red M-2BE (λ_{max} 505 nm)	
Auxiliary chemicals	
Na_2SO_4	100
NaCl	100
Na_2CO_3	150
CH_3COONa	300
CH_3COOH	100
pH[a]	7.0

[a]pH of the solution was adjusted with 0.10 mol L^{-1} NaOH and/or 0.10 mol L^{-1} HCl

Suppl. Table 5. Matrices of ANN optimized structure weights

Weights and biases between input and hidden layers						
Neuron of hidden layer	Variable					Bias
	Dye concentration	Adsorbent dose	pH	Temperature	Time	
1	−0.5298	1.6597	2.2038	3.6693	6.4779	7.5571
2	2.3907	0.5806	−2.3732	−0.7074	3.3061	3.1820
3	0.7599	−2.6249	−0.4334	1.0531	0.4612	0.8061
4	0.6598	0.5857	0.9911	−0.2316	0.4297	−0.4659
5	−2.5636	−2.7294	−0.5770	−1.3611	0.5990	−0.1203
6	−0.5802	0.8573	0.6251	1.0569	1.5337	−1.4899
7	0.1376	16.6474	4.6399	0.0353	32.7705	16.0038
8	0.9121	−1.2547	0.3630	−0.6373	2.3890	3.2310
9	1.6592	−0.3861	−1.7417	−2.2019	−3.9594	−3.9745
10	1.1976	−0.4064	−0.1209	−0.0503	−0.6134	2.9779
Weights and biase between hidden and output layers						
Neuron of hidden layer	Weights					Bias
1	0.6170					−0.8470
2	−1.1136					
3	3.4964					
4	−1.7625					
5	4.1683					
6	0.2332					
7	8.8530					
8	2.9933					
9	−0.2732					
10	−0.4298					